JOURNAL OF GEOPHYSICAL RESEARCH, VOL. 112, D22S15, doi:10.1029/2007JD009077, 2007

Aerosol single scattering albedo estimated across China from a combination of ground and satellite measurements

Kwon Ho Lee,[1] Zhanqing Li,[1,2] Man Sing Wong,[1] Jinyuan Xin,[3] Yuesi Wang,[3] Wei-Min Hao,[4] and Fengsheng Zhao[5]

Received 15 June 2007; revised 14 September 2007; accepted 26 September 2007; published 3 November 2007.

[1] Single scattering albedo (SSA) governs the strength of aerosols in absorbing solar radiation, but few methods are available to directly measure this important quantity. There currently exist many ground-based measurements of spectral transmittance from which aerosol optical thickness (AOT) are retrieved under clear sky conditions. Reflected radiances at the top of the atmosphere as measured by a spaceborne spectroradiometer are sensitive to both AOT and SSA. On the basis of extensive radiative transfer simulations, it is demonstrated that the combined use of the two measurements allows for the retrieval of SSA at a reasonable accuracy under moderate to heavy aerosol loadings. Retrieval of SSA is most sensitive to AOT and surface reflectance. The accuracy of SSA retrievals increases with aerosol loading. The uncertainties in SSA retrievals are 0.02 $\sim$ 0.03 for AOT = 1.0 and 0.03 $\sim$ 0.05 for AOT = 0.5 at 0.47 μm. The proposed retrieval method is applied to 1 a worth of Moderate Resolution Imaging Spectroradiometer (MODIS) Level-1 calibrated reflected radiances matched with surface spectral transmittances acquired at 24 stations of the Chinese Sun Hazemeter Network established under the auspices of the East Asian Study of Tropospheric Aerosols: An International Regional Experiment (EAST-AIRE). Measurements made under high-turbidity conditions (AOT > 0.4) were used. All the stations are located in relatively remote and thus spatially representative locations. From the retrieved values, the first gross map of SSA across China is generated. The retrieved SSA values were compared with those retrieved independently from AERONET sites in China. The root-mean-square deviation (RMSD) is on the order of 0.03, and the mean difference is $\sim$0.02. The nationwide means of AOT, Ångström exponent, and SSA (at 0.5 μm) in 2005 are 0.69 $\pm$ 0.17, 1.06 $\pm$ 0.26, and 0.89 $\pm$ 0.04, respectively.

Citation: Lee, K. H., Z. Li, M. S. Wong, J. Xin, Y. Wang, W.-M. Hao, and F. Zhao (2007), Aerosol single scattering albedo estimated across China from a combination of ground and satellite measurements, *J. Geophys. Res.*, *112*, D22S15, doi:10.1029/2007JD009077.

1. Introduction

[2] Atmospheric aerosols are known to influence the propagation of solar radiation in the atmosphere. The radiative forcing by atmospheric aerosols is strongly dependent upon the aerosol optical thickness (AOT, τ) and single-scattering reflectance (SSA, ω_0), which are two column-integrated quantities measuring aerosol light extinction and aerosol absorption, respectively. SSA is a key variable in assessing the climatic effect of aerosols. For example, *Hansen et al.* [1997] noted that a change in SSA from 0.9 to 0.8 can often change the sign of radiative forcing from negative to positive, depending on the reflectance of the underlying surface and the altitude of the aerosols. In addition, strongly absorbing aerosols may have a large impact on regional climate and the hydrological cycle by heating the atmosphere [*Ramanathan et al.*, 2001; *Menon et al.*, 2002]. Accurate estimation of aerosol SSA is fundamental for climate studies.

[3] Various methods have been proposed to obtain SSA using broadband solar radiative flux measurements [*Herman et al.*, 1975], spectral Sun/sky measurements [*Dubovik et al.*, 2000], spectral direct and total broadband solar radiation measurements [*Zhao and Li*, 2007], UV radiation measurements [*Petters et al.*, 2003], spaceborne measurements [*Kaufman*, 1987; *Kaufman et al.*, 2002; *Yang and Gordon*, 1998; *Wang and Gordon*, 1993; *Torres et al.*, 2005; *Hu et al.*,

[1]Earth System Science Interdisciplinary Center, Department of Atmospheric and Oceanic Science, University of Maryland, College Park, Maryland, USA.
[2]Also at Institute of Atmospheric Physics, Chinese Academy of Sciences, Beijing, China.
[3]Institute of Atmospheric Physics, Chinese Academy of Sciences, Beijing, China.
[4]Fire Science Research Lab, Forestry Service, U.S. Department of Agriculture, Missoula, Montana, USA.
[5]National Satellite Meteorological Center, China Meteorological Administration, Beijing, China.

0148-0227/07/2007JD009077$09.00

2007], direct measurements of light absorption [*Moosmüller et al.*, 1998], transmittance/scattering [*Radke et al.*, 1991; *Devaux et al.*, 1998; *Krotkov et al.*, 2005], and calculation from the Mie theory using data from chemical analyses of aerosol composition and its size distribution [*Ackerman and Toon*, 1981; *Li and Okada*, 1999]. All these methods require accurate calibration of radiation measurements and sound treatment of unknown optical properties of aerosols, surface reflectivity, and gaseous absorption.

[4] Aerosols originating from anthropogenic pollution, as well as biomass burning, in Asia are recognized as important sources of regional and global-scale pollution [*Streets et al.*, 2000; *Wenig et al.*, 2003; *Lee et al.*, 2005, 2006, 2007]. Dust storms originating from deserts occur frequently depending on meteorological conditions, and affect radiative forcing and air quality over large areas [*Takemura et al.*, 2003; *Lee et al.*, 2004; *Huang et al.*, 2006]. Asian dust from northern China can be mixed with air pollutants depending on its pathway, thus modifying its absorbing properties [*Huebert et al.*, 2003; *Seinfeld et al.*, 2004]. Furthermore, absorbing aerosols, mainly black carbon soot, can alter the regional atmospheric circulation and contribute to regional climate change in Asia [*Menon et al.*, 2002]. Although Asian aerosols are very absorbing, the spatiotemporal variability of SSA over China is largely unknown, except for a few large cities in China [*Qiu et al.*, 2004; *Zhao and Li.*, 2007]. Variation of SSA incurs large uncertainties in either remotely sensed AOT or modeling results.

[5] In this paper we propose an iterative method to retrieve SSA values by combining clear-sky measurements from ground-based spectral transmittance measurements made from a network of hazemeters (e.g., hand-held Sun photometers) and from reflected spectral radiances measured by the Moderate Resolution Imaging Spectroradiometer (MODIS). The retrievals are performed by means of radiative transfer simulations using the Santa Barbara Discrete Atmospheric Radiative Transfer (SBDART) model [*Ricchiazzi et al.*, 1998]. SBDART uses a numerically stable solver for plane-parallel radiative transfer in a vertically inhomogeneous atmosphere. The retrieved SSA values are then compared to Aerosol Robotic Network (AERONET) inverted products [*Dubovik et al.*, 2002]. The new method is applied to the matched ground-based and satellite data acquired at 24 stations across China for the year 2005 to gain a sense of the gross spatial and temporal distributions of SSA.

[6] This paper is organized as follows. Sections 2 and 3 describe the data set used to retrieve the SSA and the details of the retrieval algorithm. Section 4 presents the sensitivity tests of the retrieval method. The results of SSA retrievals at all hazemeter stations and their consistency with AERONET data are discussed in section 5. Finally, the conclusions of the study are summarized in section 6.

2. Data Set

[7] The data sets used in this study include ground-based measurements from the Chinese Sun-Hazemeter Network (CSHNET) established under the auspices of the East Asian Study of Tropospheric Aerosols: an International Regional Experiment (EAST-AIRE) [*Li et al.*, 2007a; *Xin et al.*, 2007], MODIS Level-1 (L1) calibrated radiance data, and AERONET Sun photometer data (http://aeronet.gsfc.nasa.gov). Figure 1 shows the locations of the Sun hazemeter and some AERONET sites selected for the consistency checks.

[8] The Sun hazemeters, which are in operation at 24 sites in China and are taking measurements more than 20 times a day (the observation period is from 1000 to 1400 local time), provide AOT data at four spectral wavelengths (405 nm, 500 nm, 650 nm, and 880 nm). The Sun hazemeters were manufactured by the United States Department of Agriculture (USDA) Forestry Service and has been used to estimate AOT [*Hao et al.*, 2005; *Yamasoe et al.*, 2006; *Xin et al.*, 2007]. Langley plot and transfer calibration methods were used for calibrating the Sun hazemeters [*Brooks and Mims*, 2001; *Xin et al.*, 2007]. Sun hazemeter data are generally consistent with AERONET CIMEL Sun photometer results with disagreements on the order of 2% to 6%. Larger errors of 12 $\sim$ 15% at 880 nm were found and are due to the large full-width half-maximum (30 nm) at that wavelength, water vapor contamination and observation errors [*Xin et al.*, 2007]. Measurements from this channel are thus not employed in this study. Since the Sun hazemeter only measures direct solar radiation, retrievals of other aerosol optical properties, such as SSA, are not available.

[9] The 1-km resolution TERRA/MODIS L1 data (collection 5) obtained from NASA (http://ladsweb.nascom.nasa.gov/) were used to calculate aerosol path radiance (ρ_{aer}). The MODIS L1 data at two visible bands and one shortwave infrared band (0.47 μm, 0.66 μm, and 2.1 μm), well known for aerosol retrievals over land [*Kaufman et al.*, 1997; *Levy et al.*, 2007], are used to estimate the ρ_{Aer}. Data from more MODIS channels are employed to choose clear-sky pixels following the MODIS clear-sky discriminating method [*Ackerman et al.*, 1998].

[10] Additionally, CIMEL Sun photometer–based aerosol optical and physical parameter data from four AERONET sites in China (Beijing: 116.381°E, 39.977°N; Hefei: 117.162°E, 31.905°N; Taihu: 120.215°E, 31.421°N; Xianghe: 116.962°E, 39.754°N) were used for consistency checks of the SSA retrieval results, together with six AERONET sites of heavy aerosol loadings in other countries (Kanpur: 80.346°E, 26.450°N; Ispra: 8.627°E, 45.803°N; GSFC: −76.840°E, 38.992°N; Llorin: 4.34°E, 8.32°N; Ougadougou: −1.40°E, 12.20°N, and Djougou: 1.599°E, 9.760°N). At these AERONET sites, spectral AOTs and SSAs are derived from Cimel Sun photometer measurements of direct Sun beam and aureole radiances following the inversion algorithm of *Dubovik and King* [2000]. Quality-assured Level 2.0 AERONET data (version 2.0) are used to estimate the optical and microphysical properties of atmospheric aerosols in this study.

3. Methodology

[11] The SSA retrieval method minimizes the differences between calculated and measured ρ_{Aer}. It is different from the inversion method using spectral and scattering angle–dependent measurements. Essentially, the hazemeter measures total aerosol loading or AOT, while satellite measured radiances at top-of-the-atmosphere (TOA) provide information pertaining to aerosol scattering, assuming other con-

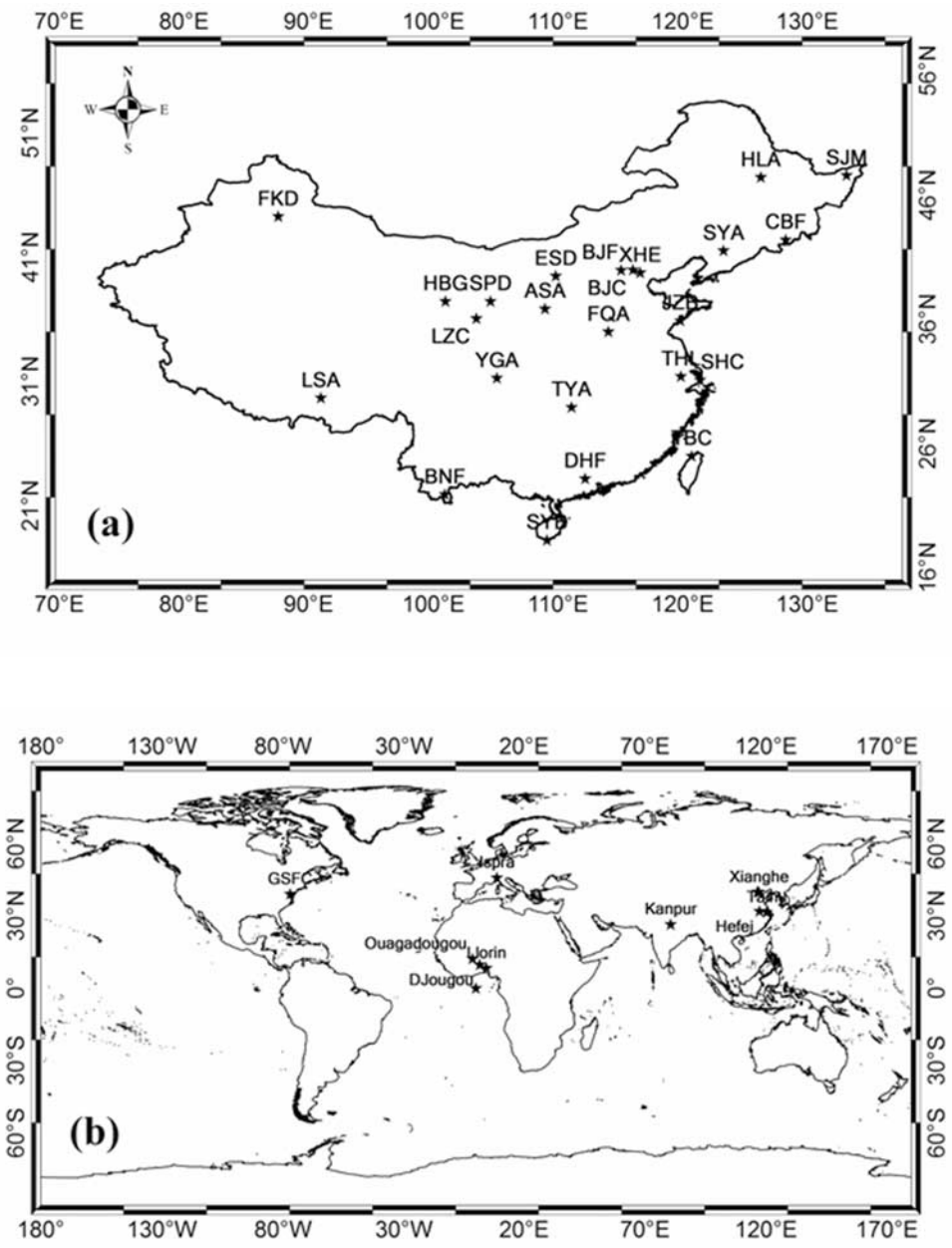

Figure 1. Location of (a) 24 Sun hazemeter sites and (b) 10 AERONET sites used in this study. Note that the location of Sun hazemeter sites is the same as those from the Chinese Sun Hazemeter Network (CSHNET) listed by *Xin et al.* [2007, Table 1]. Three additional sites (Taibei, 121.09°E, 25.00°N; Dinghu Mt.,112.53°E, 23.17°N; and Sanya, 109.47°E, 18.22°N) are used in this study.

tributions due to surface reflection and molecular scattering are corrected. In addition to TOA reflected radiances and AOT, the Ångström exponent (α) is also used in our retrieval, as it is governed by aerosol particle size.

[12] The SSA retrieval algorithm is composed of three parts, as shown in Figure 2. First, RTM input data are computed from the MIE theory for assumed refractive index and the Junge power law size distribution determined for different values of the Ångström exponent. Then reflectance at the top of the atmosphere $\rho_{\mathrm{TOA}}(\lambda)$ in the MODIS bands are calculated with aerosol properties from ground-based transmittance measurement and MODIS viewing geometry. Second, aerosol path reflectances ($\rho_{aer}(\lambda)$) are determined by removing the contributions of Rayleigh scattering ($\rho_{Ray}(\lambda)$) and surface reflectance ($\rho_{Surf}(\lambda)$) for cloud-free pixels.

$$\rho_{aer}(\lambda) = \rho_{TOA}(\lambda) - \rho_{Ray}(\lambda) - \frac{T_{Sun}(\lambda) \cdot T_{Sat}(\lambda) \cdot \rho_{surf}(\lambda)}{1 - s \cdot \rho_{surf}(\lambda)} \quad (1)$$

where T is atmospheric transmittances for direct and diffuse radiances (T_{Sun} *and* T_{Sat}), and s is hemispheric albedo. Finally, SSA is retrieved by minimizing differences between

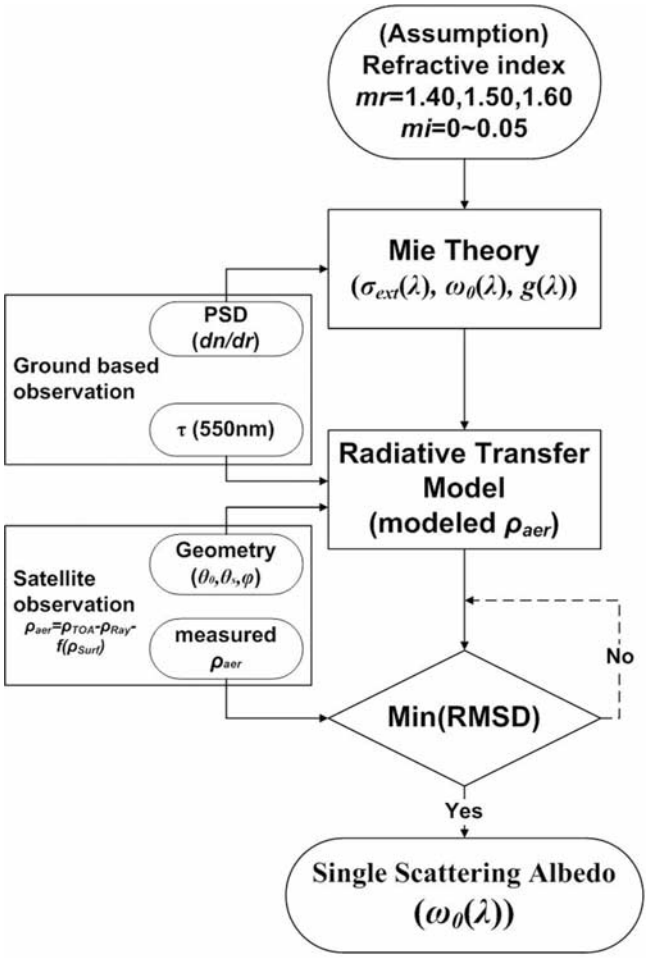

Figure 2. Schematic diagram of the SSA retrieval method.

measured and calculated ρ_{aer} in terms of the root mean square difference (RMSD) which is defined as:

$$RMSD(\lambda_i) = \sqrt{\left(\frac{\rho^m_{aer}(\lambda_i) - \rho^c_{aer}(\lambda_i)}{\rho^m_{aer}(\lambda_i)}\right)^2} \quad (2)$$

where ρ^m_{aer} and ρ^c_{aer} are measured and calculated aerosol reflectances, respectively. RMSD calculations were done at the selected wavelengths of 0.47 μm and 0.66 μm for MODIS bands 3 and 1, independently.

[13] For the calculation of ρ_{aer}, the SBDART radiative transfer code was run using the following input parameters: the standard model atmosphere, aerosol optical parameters (extinction cross section, SSA, asymmetry parameter) determined from the Mie theory [*Bohren and Hoffman*, 1983], AOTs measured with hazemeters, and geometry from MODIS geometry data (MOD03). SSA is determined by varying the refractive indices (m_r = 1.4, 1.5, and 1.6 with $m_i = 0 \sim 0.010$ ($\Delta = 0.001$) and 0.010~0.050 ($\Delta = 0.002$)) until the best agreement is found between modeled and measured radiances, i.e., RMSD reaches minimum. To better resolve the angular dependence of the radiation field, 8-stream mode was used [*Stamnes et al.*, 1988].

[14] Sun hazemeter data were averaged within 30 min of the MODIS overpass times. The Ångström exponent was determined using the log linear fitting ($r > 0.9$) of wavelength-dependent AOT values at three wavelengths (405 nm, 500 nm, and 650 nm) [*Lee et al.*, 2005]. Using these Ångström exponent values, AOT at 550 nm was derived. These data were used as input for the RTM.

[15] MODIS data were averaged within a 20-km radius [*Kovacs*, 2006] around the location of each Sun hazemeter station. Rayleigh scattering is removed from TOA reflectances for each pixel using an equation in the work by *Bucholtz* [1995]. Surface reflectances at 0.47 μm and 0.66 μm are determined from reflectance at 2.12 μm. In the previous version of the algorithm (Version 4), fixed empirical ratios ($\rho_{0.47} = 0.25 \times \rho_{2.12}$ and $\rho_{0.66} = 0.5 \times \rho_{2.12}$) [*Kaufman et al.*, 1997] were used. The most recent version of the algorithm (Version 5) accounts for the dependence of the ratios on the normalized difference vegetation index and scattering angle [*Levy et al.*, 2007]. These ratios are useful in global-scale surface reflectance determination because the ratios are highly dependent on land cover type and the temporal variation of vegetation. In this study, the ratios are obtained at each site under low aerosol-loading conditions (AOT < 0.2), following atmospheric correction [*Li et al.*, 2007b]. Then surface reflectance at two visible MODIS bands were determined by applying these ratios to ordinary conditions of aerosol loading.

4. Uncertainty/Sensitivity Analysis

[16] The aerosol models from OPAC 3.1 [*Hess et al.*, 1998] were used for the sensitivity analysis of the SSA retrieval. Table 1 summarizes the microphysical parameters of four different aerosol models (CA; Continental Average, UB; Urban, DD; Desert Dust, MC; Maritime Clean). Errors in either aerosol data or surface reflectance data can produce errors in the retrieval of SSA. The uncertainty analysis for each of the retrieval-related factors is given below and summarized in Table 2.

4.1. AOT

[17] Figure 3 shows ρ_{aer} calculated with different SSA values (0.7 ~ 1.0, step size = 0.01) and AOTs (0.0 ~ 3.0, step size = 0.01) for the four different aerosol models at 0.47 μm and 0.66 μm. The standard deviations of ρ_{aer} were also obtained from the ρ_{aer} for different aerosol models at a given AOT and SSA. In general, ρ_{aer} is quite sensitive to SSA as AOT increases. However, ρ_{aer} is not as sensitive to SSA when aerosol loading is low. This implies that the accuracy of the SSA retrieval increases with aerosol loading. Therefore SSA retrievals can only be made under high aerosol loading conditions, as is often found in many locations in China [*Xin et al.*, 2007]. This result is similar to that found by *Dubovik et al.* [2000] and *Zhao and Li* [2007] using different retrieval methods.

4.2. Size Distribution

[18] The aerosol particle size distribution (PSD) is another key parameter in determining aerosol optical properties in radiative transfer calculations. Errors arise when certain assumptions regarding the PSD are not correct. Two

Table 1. Microphysical and Optical Properties of Aerosol Models Used in This Study [From *Hess et al.*, 1998, Table 1c]

Aerosol Types	Aerosol Components	Number Density, n_i,[a] cm^{-3}	r_{medN}, μm	σ	r_{eff}, μm
Continental average (CA)	water-soluble	7,000	0.0212	2.24	0.18
Continental average (CA)	insoluble	0.4	0.471	2.51	0.18
Continental average (CA)	soot	8,300	0.0118	2	0.18
Urban (UB)	water-soluble	28,000	0.0212	2.24	0.12
Urban (UB)	insoluble	1.5	0.471	2.51	0.12
Urban (UB)	soot	130,000	0.0118	2	0.12
Desert dust (DD)	water-soluble	2,000	0.0212	2.24	1.08
Desert dust (DD)	mineral (nuc.[b])	269.5	0.07	1.95	1.08
Desert dust (DD)	mineral (acc.[c])	30.5	0.39	2	1.08
Desert dust (DD)	mineral (coa.[d])	0.142	1.9	2.15	1.08
Maritime clean (MC)	water-soluble	1,500	0.0212	2.24	0.43
Maritime clean (MC)	sea salt (acc.)	20	0.209	2.03	0.43
Maritime clean (MC)	sea salt (coa.)	3.2×10^{-3}	1.75	2.03	0.43

[a] n_i, number of particles of i-component.
[b] nuc., nucleation mode.
[c] acc., accumulation mode.
[d] coa., coarse mode.

commonly used PSD functions are employed to test its sensitivity, namely, the lognormal size distribution:

$$\frac{dN_i(r)}{dr} = \frac{N_i}{\sqrt{2\pi}\cdot r \log\sigma_i \cdot \ln 10} \exp\left[-\frac{1}{2}\left(\frac{\log r - \log r_i}{\log \sigma_i}\right)^2\right] \quad (3)$$

and the Junge power law size distribution:

$$\begin{aligned} \frac{dN(r)}{dr} &= K,\ (0.03\ \mu\text{m} < r \le 0.1\ \mu\text{m}) \\ &= K\cdot\left(\frac{0.1}{r}\right)^{\upsilon+1},\ (0.1\ \mu\text{m} < \text{r} \le 10\ \mu\text{m}) \\ &= 0,\ (\text{r} > 10\ \mu\text{m}) \end{aligned} \quad (4)$$

where υ is (α + 2) and K is a constant. Using these aerosol models, satellite-measured radiances under specific AOT and SSA conditions can be derived.

[19] In Figure 4, the differences between SSA derived from the two PSD functions (power law and lognormal distribution) are shown. The Ångström exponents, which are used as a Junge distribution parameter (υ) for each aerosol model, are 1.42 (CA), 1.43(UB), 0.17(DD), and 0.08(MC) [*Hess et al.*, 1998]. The MC model has the largest discrepancies at both wavelengths (up to 0.027 at 0.47 μm and 0.045 at 0.66 μm). The DD model also shows larger discrepancies than the other two models; the UB model has the smallest differences. This suggests that the power law does not describe the PSD containing large particles very well. Since SSA retrievals in this study are carried out over land, errors caused by the MC model are not as much of a concern as those from the DD model. The SSA differences decrease as AOT increases in each plot of Figure 4. Table 3 shows errors resulting from the choice of PSD and surface reflectance. The decreasing rate of SSA differences as a function of AOT ($\Delta\omega_0/\Delta\tau \times 100$) are 40 $\sim$ 78% (CA), 33 $\sim$ 47% (DD), and 5 $\sim$ 28% (MC), respectively.

[20] *Hansen and Travis* [1974] showed that for a fixed refractive index, the phase functions computed for significantly different size distributions are similar as long as the size distributions have the same effective radius, r_{eff}, and effective variance, v_{eff}, given by

$$r_{eff} = \frac{\int r^3 \cdot N(r)dr}{\int r^2 \cdot N(r)dr} \quad (5)$$

and

$$v_{eff} = \frac{\int \left(r - r_{eff}^2\right)^2 \cdot r^2 \cdot N(r)dr}{r_{eff}\int r^2 \cdot N(r)dr} \quad (6)$$

[21] In these simulations, the same effective radius (r_{eff} = 0.1, 0.5, 1.0, 2.0, 5.0 μm) and effective variance (v_{eff} = 0.61) for different aerosol size distribution function are used. Figure 5 shows that in general, the difference in SSA between the lognormal and the Junge power law SDF increases as the effective radius increases (for $r_{eff} < 5$ μm); the differences are at their minimum values where r_{eff} = 5.0 μm.

[22] Since the Ångström exponent is an important parameter in determining the Junge power law size distribution, it is one of the factors affecting SSA retrievals. Figure 6 shows the results of the sensitivity study regarding the dependence of the SSA retrieval at 0.47 μm and 0.66 μm on the Ångström exponent. From the Junge power law distributions for the Ångström exponent values (α = 0.0 $\sim$ 2.0,

Table 2. Uncertainty of Input Parameters and Retrieval Errors

Parameter	Uncertainty	Error
Hazemeter AOT	2 $\sim$ 6%	±0.04
PSD		±0.02
Ångström	10%	±0.02
Surface reflectance	±0.01	±0.10
Vertical distribution		±0.005
Shape		±0.03
Refractive index	mr	±0.05
Refractive index	mi	±0.06
Sensor calibration	1.5 $\sim$ 5%	±0.01
Combined		±0.21

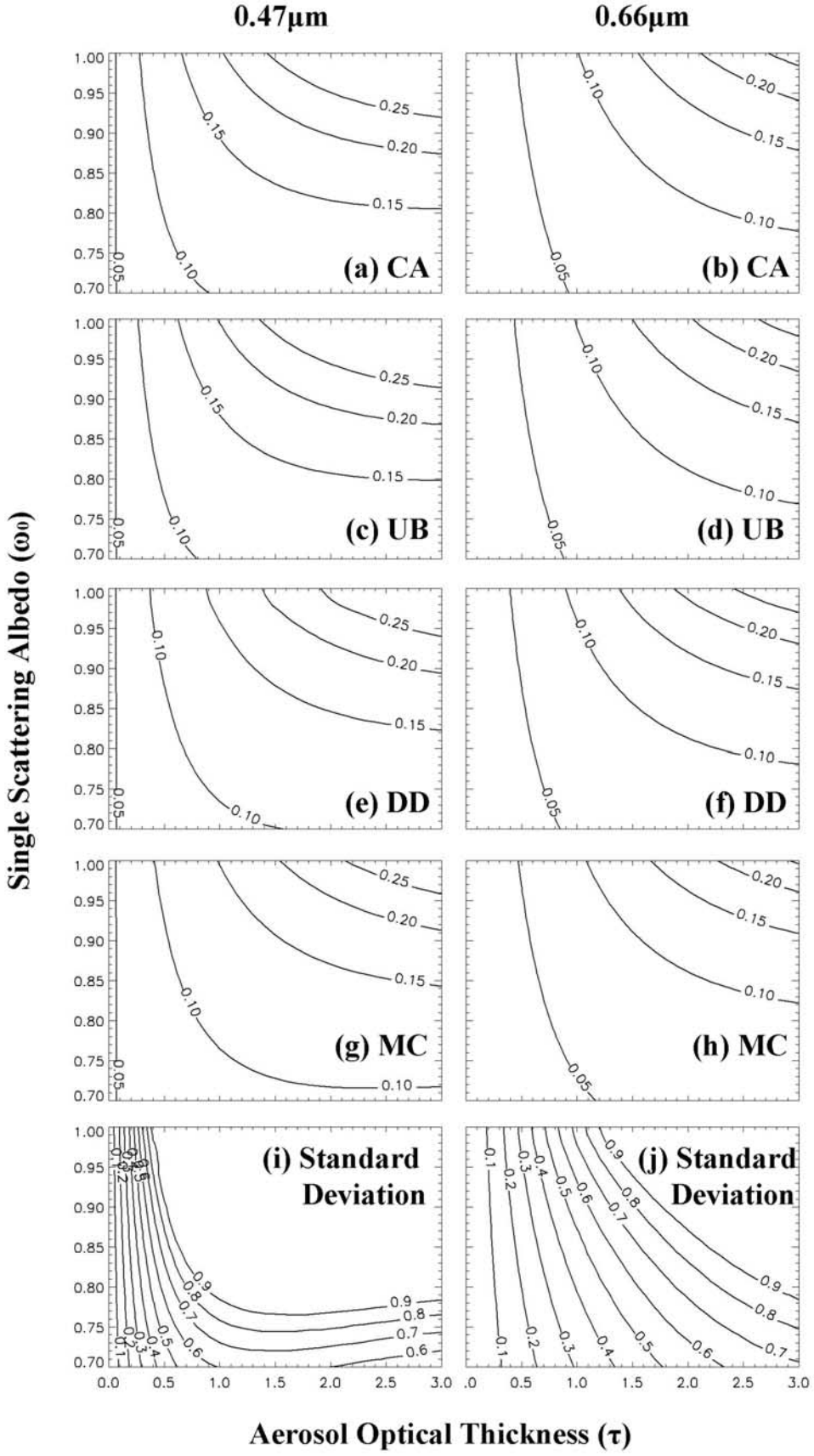

Figure 3. (a–h) Aerosol path radiances and (i and j) the standard deviation ($\times 100$) as a function of AOT and SSA for different aerosol models from Table 1. Other inputs to the RTM are $\rho_{\mathrm{Surf}} = 0.0$, $\theta_0 = 40$, $\theta_s = 20$, and $\varphi = 0$.

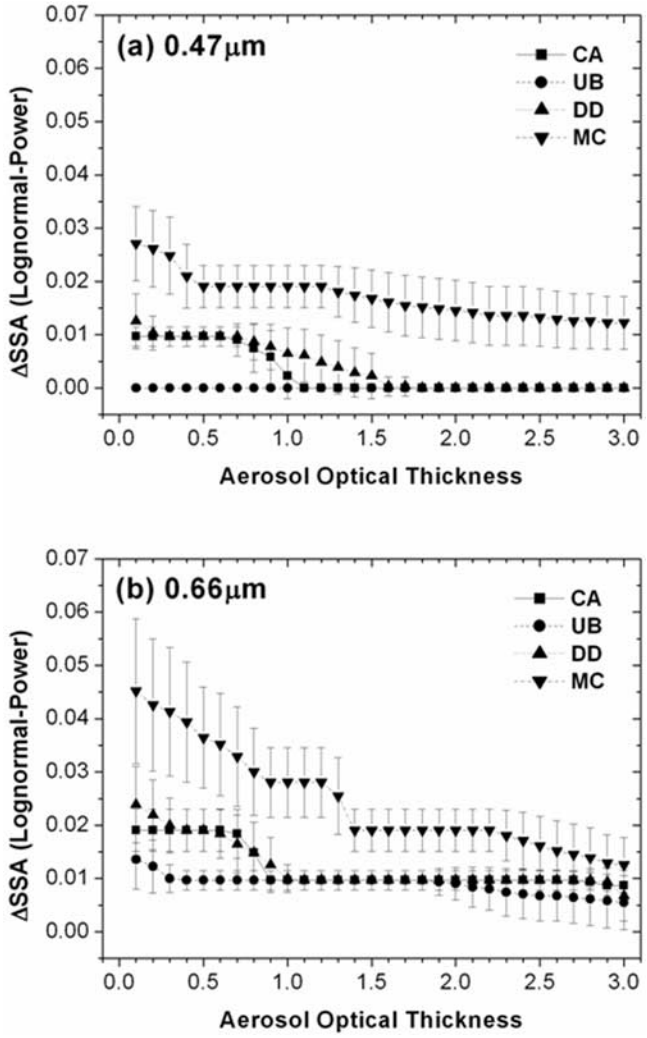

Figure 4. Differences in SSA ($\Delta\omega_0$) at (a) 0.47 μm and (b) 0.66 μm between the lognormal and Junge power law size distributions. The Ångström exponents, as a Junge distribution parameter (υ) for each aerosol model, are 1.42 (CA), 1.43(UB), 0.17(DD), and 0.08(MC), respectively [*Hess et al.*, 1998].

step size = 0.1), the effect of the aerosol size distribution on SSA as a function of AOT and the Ångström exponent was estimated. The contour lines in Figure 6 denote the SSA retrieval errors resulting from a ±0.1 change with Ångström exponent. An error of ±0.1 in the Ångström exponent would lead to maximum retrieval errors in SSA of 0.021 at 0.47 μm and 0.013 at 0.66 μm.

4.3. Surface Reflectance

[23] It follows from equation (1) that surface reflectance is needed to separate aerosol contributions from the total observed atmospheric path radiance. The sensitivity of SSA retrievals to surface reflectance is thus investigated. Surface reflectance is determined following *Levy et al.* [2007]. A comparison between MODIS-retrieved and atmospherically corrected surface reflectances shows uncertainties of 0.006 at 0.47 μm and 0.017 at 0.66 μm in surface reflectance [*Li et al.*, 2007b]. The relationship between surface reflectance and SSA was calculated using the four different aerosol models outlined in Table 1. As shown in Figure 7 and summarized in Table 3, a significant error in SSA may be incurred by an error of ±0.01 in the surface reflectance for small AOT. For AOT = 0.5, the error in SSA ranges from 0.037 to 0.061 at 0.47 μm and from 0.077 to 0.089 at 0.66 μm. These errors decrease as AOT increases, as shown in Figure 7 and described by the exponential function given in Table 3 (the last rows). Because of the high sensitivity, this method is only valid over regions of high aerosol loading also.

4.4. Vertical Distribution

[24] The vertical distribution of aerosol properties is a key parameter required for computing radiative properties [*Wendisch et al.*, 1996; *Haywood and Ramaswamy*, 1998]. It is also important to estimate SSA because it influences ρ_{aer}. To test the sensitivity of the aerosol vertical distribution to the SSA retrieval, five vertical distributions of absorbing aerosol density are assumed and are shown in Figure 8a. For these aerosol vertical distributions, we calculated the dependence of the SSA on the height of the absorbing aerosol layer using the SBDART code. Figure 8b shows the dependence of the errors in SSA ($\Delta\omega_0$) at 0.47 μm and 0.66 μm and Rayleigh scattering, as a function of height, for three AOT values. The SSA error due to the changes of ±1 km is defined as the difference between the SSA value at z km and $z \pm 1$ km. The errors are less than 0.015 at 0.47 μm and less than 0.001 at 0.66 μm and are strongly affected by Rayleigh scattering.

4.5. Particle Shape, Sensor Calibration, Refractive Index, and Relative Humidity

[25] Spherical particles are assumed in the development of our retrieval algorithm. It is important to consider the influences of nonspherical particles, such as mineral dust, in computing aerosol optical properties. On the other hand, information on aerosol type is highly limited. As a sensitivity test, we employed different particle phase functions

Table 3. Errors in the Retrieved SSA Due to Particle Size Distribution (PSD) and Surface Reflectance[a]

	Wavelength	CA	UB	DD	MC
		PSD (Power Law Versus Lognormal)			
τ = 0.5	0.47	0.009	0.000	0.009	0.019
τ = 0.5	0.66	0.015	0.009	0.019	0.036
τ = 1.0	0.47	0.002	0.000	0.006	0.018
τ = 1.0	0.66	0.009	0.009	0.010	0.026
		ρ_{surf} *(±0.01)*			
τ = 0.5	0.47	0.037	0.037	0.053	0.061
τ = 0.5	0.66	0.089	0.085	0.074	0.088
τ = 1.0	0.47	0.011	0.010	0.019	0.019
τ = 1.0	0.66	0.029	0.028	0.023	0.028
		$y^b = a \cdot exp[-x/t]$			
a	0.47	0.212	0.210	0.202	0.201
t	0.47	0.297	0.291	0.397	0.428
a	0.66	0.204	0.203	0.195	0.204
t	0.66	0.589	0.579	0.490	0.579

[a]Note that the error caused by ±0.01 surface reflectance decreases when AOT increases as shown in Figure 7. These errors are fit by the exponential function given in the last row of the table.
[b]y, SSA error by surface reflectance; x, AOT.

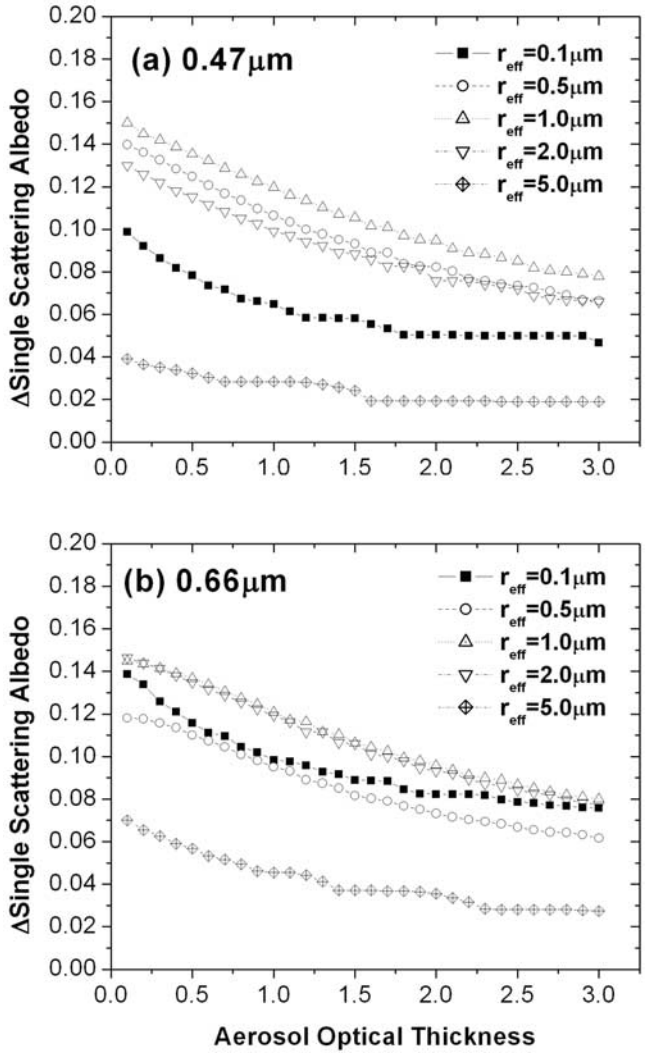

Figure 5. Differences between the lognormal and Junge power law size distributions in SSA ($\Delta\omega_0$) due to changes in effective radius (r_{eff}) at (a) 0.47 μm and (b) 0.66 μm channels. Other inputs to the Mie scattering calculation are fixed with effective variance $v_{eff} = 0.61$. Spectral refractive indices of soot particle are taken from *Hess et al.* [1998].

from *Lee et al.* [2007] that were obtained from the Mie scattering theory for spherical particles and the T-Matrix code [*Mishchenko and Travis*, 1998] for nonspherical dust particles. SSA errors caused by the shape difference are estimated to be less than 0.059 at 0.47 μm and 0.064 at 0.66 μm.

[26] Estimation of ρ_{aer} may contain a systematic error due to an instrumental calibration error. Per the uncertainty index table from the MODIS Level 1B Product User's Guide, a range of uncertainty, 1.5 $\sim$ 5%, is considered. The resulting SSA retrieval error is very small: 0.0003 $\sim$ 0.028.

[27] Retrieval of SSA is sensitive to both the real part as well as the imaginary part of the refractive index. As shown in Figure 9, TOA reflectance strongly depends on both parts of refractive index. The retrieval error in SSA caused by the real (1.5 ± 0.1) and imaginary part (± 0.01) are less than 0.04 and 0.05 respectively. Although the imaginary part of a refractive index represents light absorption of particles, the real part is also important in this retrieval because satellite-measured TOA reflectance is affected by the scattered radiation.

[28] The impact of aerosol humidity, or the swelling effect, on SSA retrievals is difficult to assess. Humidity growth is a complicating factor when trying to characterize aerosol size distributions from satellites [*Kapustin et al.*, 2006], although it has been studied extensively using ground-based and airborne data [e.g., *Jeong et al.*, 2007]. The degree of hygroscopic growth and the resulting changes in aerosol optical properties are functions of particle composition, size and shape. As the particle size grows, particle scattering increases, and SSA increases. Since the impact is exerted on both upward and downward measurements, the retrieval algorithm will partially account for its influence. No doubt, this factor contributes to some of the SSA variability as discussed below.

5. Results

[29] In almost all sensitivity tests, the uncertainties of SSA retrievals increase with AOT. Therefore SSA is

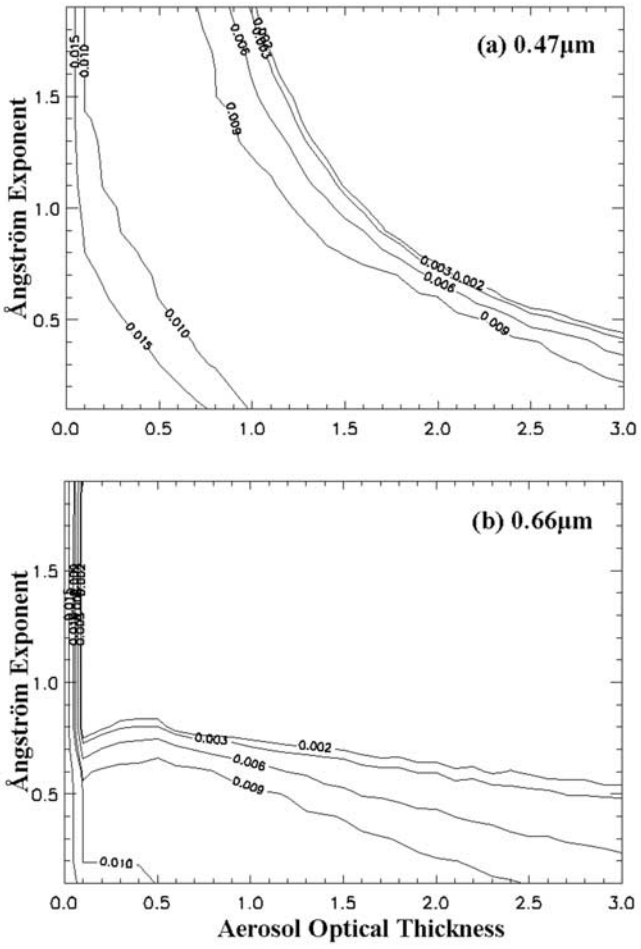

Figure 6. Errors in SSA ($\Delta\omega_0$) due to a 10% change in the Ångström exponent at (a) 0.47 μm and (b) 0.66 μm channels.

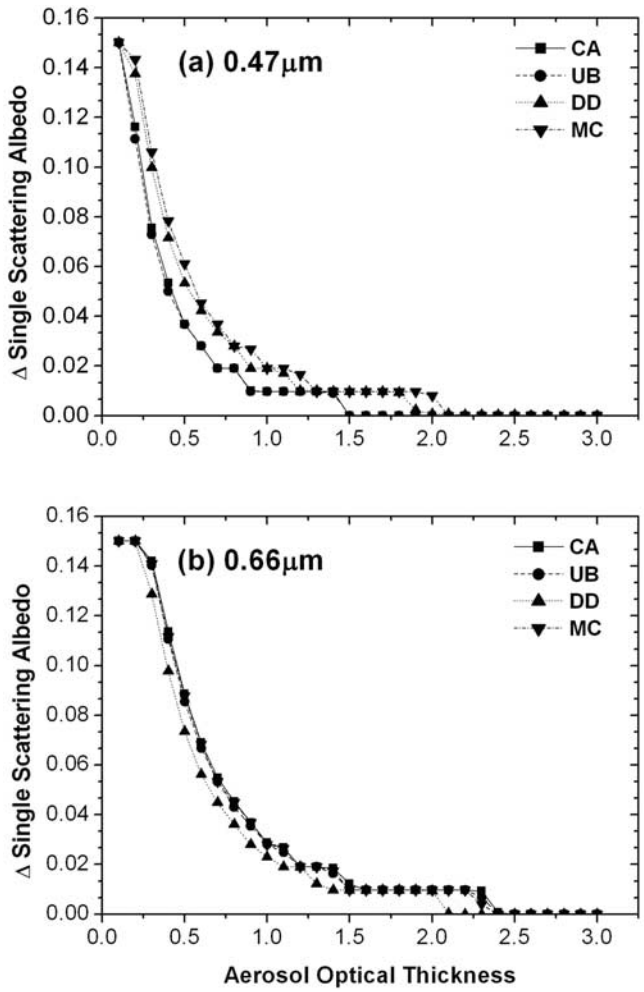

Figure 7. Errors in SSA ($\Delta\omega_0$) at (a) 0.47 μm and (b) 0.66 μm caused by an error of ±0.01 in surface reflectance (ρ_{surf}).

retrieved only for AOT > 0.4 in this study. The SSA retrieval results were compared with those from AERONET shown in Figure 10 for all 4 AERONET sites in China. The AERONET SSA values are calculated from the spectral measurements of direct/diffuse radiation using forward modeling and numerical inversion [*Dubovik and King*, 2000]. Errors in AERONET SSA were estimated to be around 0.03 (AOT > 0.2) and 0.05 $\sim$ 0.07 (AOT $\leq$ 0.2) [*Dubovik et al.*, 2000]. Since the AERONET SSA data were also obtained from a retrieval method, the comparison serve as a consistency check rather than a validation for which ground-truth values are required. To this end, the SSA retrieval method introduced above was applied to coincident/collocated AERONET AOT data and MODIS reflectance data that were matched following the same procedure as for matching with hazemeter data. The retrieved SSA results are then compared with the AERONET SSA retrievals.

[30] The two sets of retrievals agree to within their expected ranges of uncertainties. At two northern sites (Beijing and Xianghe), the standard deviation (SD) and mean differences (MD) are 0.029 and 0.005 at 0.47 μm, respectively, and 0.031 $\sim$ 0.036 and 0.013 $\sim$ 0.015 at 0.66 μm, respectively. Larger differences are found in Hefei and Taihu. These stations are located on lakeshores where the estimation of surface reflectance is susceptible to larger errors. The discrepancies may originate from the surface reflectance correction used to obtain path radiances, averaging of pixel radiances in satellite data, and the choice of the PSD. Table 4 presents a summary of all comparison results at the four AERONET sites in China, together with six AERONET sites in other countries: Kanpur, Ispra, GSFC, Llorin, Ougadougou, and Djougou. The mean values of the retrieved SSA from AERONET and the current method are shown, as well the SD and MD between the two sets of retrievals.

[31] Figure 11 presents the comparison of the seasonal means of SSA retrieved from the current method against those from the AERONET at all AERONET sites under study. Note that the plots are for SSA ranging from 0.7 to 1.0. The 1:1 line and the organic regression analysis result [*Hirsch and Gilroy*, 1984] are marked. Given the various sources of uncertainty, the agreement between the two retrievals are reasonably good, with slope = 0.96, and correlation coefficient r = 0.71 at 0.47 μm. The agreement is somewhat worse at 0.66 μm (slope = 0.82, r = 0.59). The

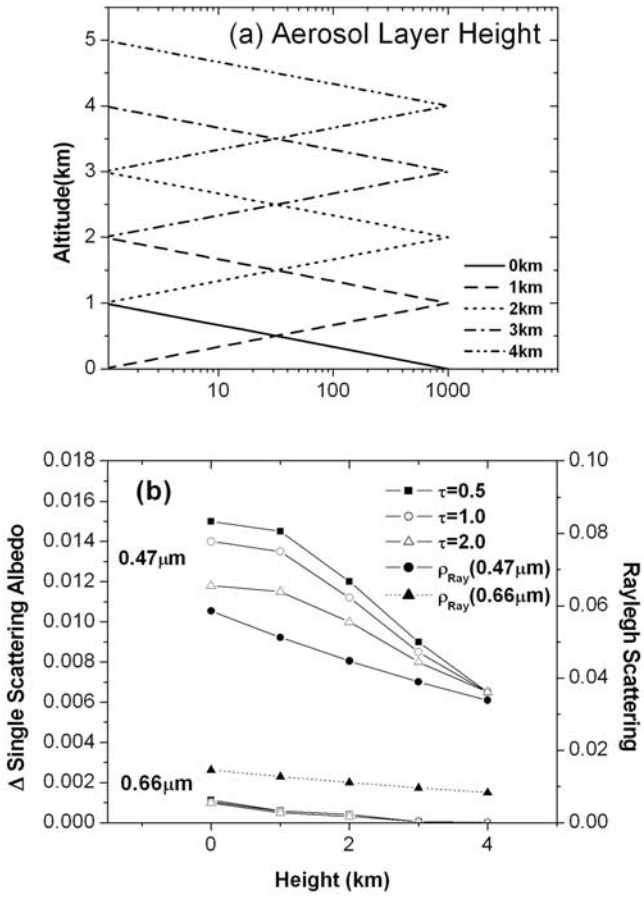

Figure 8. (a) Five assumed vertical distributions of absorbing aerosol layers (AAL). (b) Dependence of the errors in SSA ($\Delta\omega_0$) at 0.47 μm and 0.66 μm and Rayleigh scattering, as a function of height, for three AOT values.

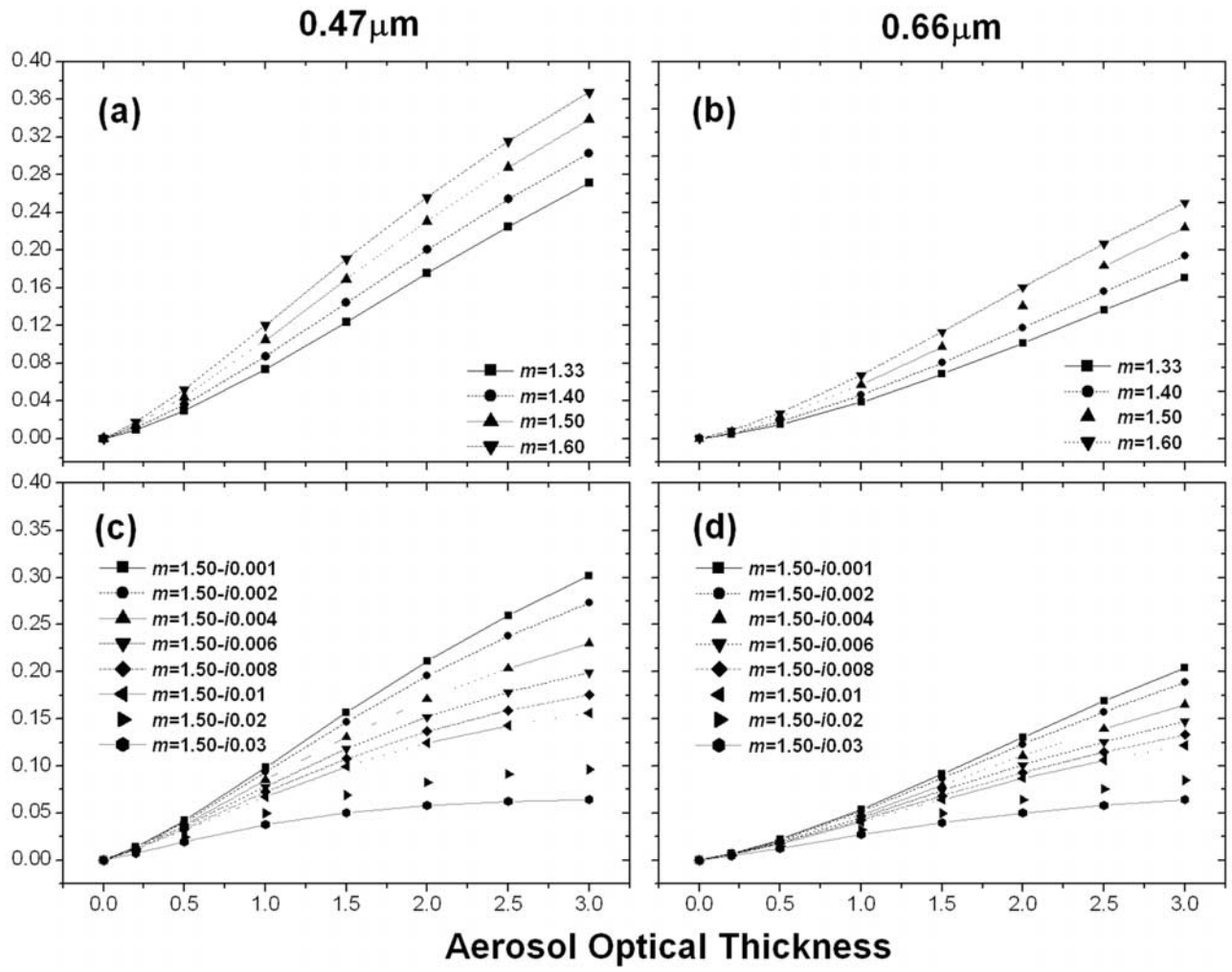

Figure 9. TOA reflectance as a function of AOT with (a and b) zero imaginary part and (c and d) fixed real part of refractive indices. Other inputs to the SBDART calculation are zero surface reflectance and size distribution from the continental average model [*Hess et al.*, 1998].

worse agreement may be due to a larger error in determining surface reflectance. Both correlations are statistically significant ($p < 0.0001$).

[32] The time series of SSA retrieved from hazemeters are also compared with those from the AERONET at two northern sites in China (Beijing and Xianghe) for the entire year of 2005, as shown in Figure 12. The day-to-day variation of SSA as retrieved from hazemeters is more or less the same as that from the AERONET retrieval at 0.47 μm at both sites. The hazemeter retrievals at 0.66 μm are slightly lower. Mean values were estimated in the range of 0.86 $\sim$ 0.88 at 0.47 μm, indicating the presence of moderately strong absorbing aerosols. Differences of 0.05 at Beijing and 0.04 at Xianghe occur at 0.66 μm. More variable surface reflectances are likely the major cause of the discrepancies.

[33] In Table 5, the seasonal and annual means of SSA values at the standard wavelength of 0.55 μm are listed and were obtained by linear interpolation from the retrieved values at wavelengths of 0.47 and 0.66 μm at all hazemeter sites. The sites are grouped into five ecosystems [*Xin et al.*, 2007]: Urban, Agriculture, Forest, Desert, and miscellaneous. In addition to SSA, the corresponding mean values of AOT and the Ångström exponent, were also calculated and listed for each station. Yearly averaged AOT varied from 0.41 (Hailun) to 0.93 (Yanting). In general, AOT over urban areas are higher than AOT values elsewhere, varying from 0.65 (Shanghai) to 0.82 (Lanzhou). This is likely due to increased anthropogenic emissions which is suggested by the large Ångström exponent (1.12) and small SSA (0.87). The lowest magnitudes in Ångström exponent (0.64) are found at the desert sites where dust aerosols are prevalent. Over the study area during 2005, the mean AOT (0.69 ± 0.17), Ångström exponent (1.07 ± 0.26), and SSA (0.89 ± 0.04) indicates that heavy aerosols (AOT > 0.4) of moderately strong absorption, dominate the atmosphere of China.

[34] Figure 13 shows the spatial distributions of SSA at 0.47 μm and 0.66 μm across China. It is worth noting that relatively large SSA over central-east China coincides with large AOT as seen from MODIS satellite retrievals [*Li et al.*, 2007b]. This region is the heart of the Chinese industrial zone and is thus likely fraught with industrial pollutants

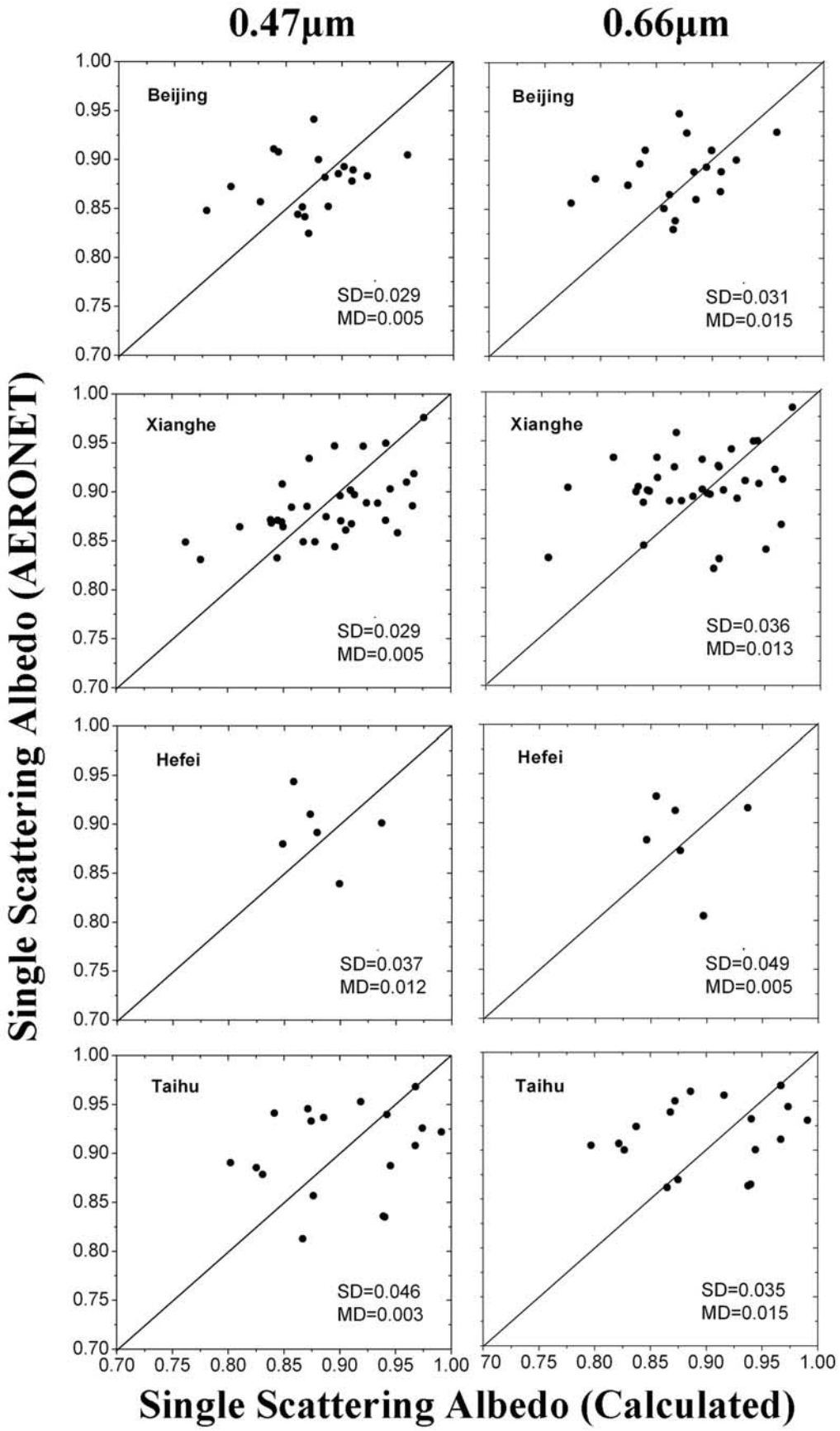

Figure 10. Comparisons between individual SSAs retrieved from this study and those from the AERONET SSA at four sites in China.

Table 4. Summary of the Comparison Results in Figures 8 and 9

	0.47 μm				0.66 μm			
	This Study	AERONET	SD	MD	This Study	AERONET	SD	MD
Beijing	0.872	0.877	0.029	0.005	0.870	0.885	0.031	0.015
Xianghe	0.891	0.886	0.029	0.005	0.889	0.902	0.036	0.013
Hefei	0.882	0.894	0.037	0.012	0.880	0.886	0.049	0.005
Taihu	0.903	0.903	0.046	0.004	0.901	0.916	0.035	0.015
Kanpur	0.895	0.885	0.031	−0.011	0.899	0.882	0.039	−0.017
Ispra	0.913	0.933	0.027	0.019	0.910	0.928	0.020	0.018
GSFC	0.931	0.950	0.019	0.019	0.928	0.938	0.023	0.011
Llorin	0.874	0.868	0.035	−0.006	0.894	0.888	0.042	−0.005
Ouagadougou	0.868	0.876	0.028	0.006	0.893	0.922	0.037	0.026
Djougou	0.860	0.863	0.036	0.001	0.871	0.902	0.044	0.029

such as sulfate. There are three regions of low SSA: northeastern China, central-north China and western China. The low SSA in northeastern China appears to be related to coal burning, which is the main source of heating, while the latter two low-SSA sites are overwhelmed by dust aerosols that are also moderately strong absorbing aerosols. Comparing the upper and lower panels, one can readily see the close similarity between SSAs retrieved at the two channels in terms of both magnitude and the spatial variation pattern. It is worth mentioning that the two retrievals are independent of each other, for they use different TOA radiances and surface reflectances. The similarity itself is a testimony to the strength of the retrieval algorithm.

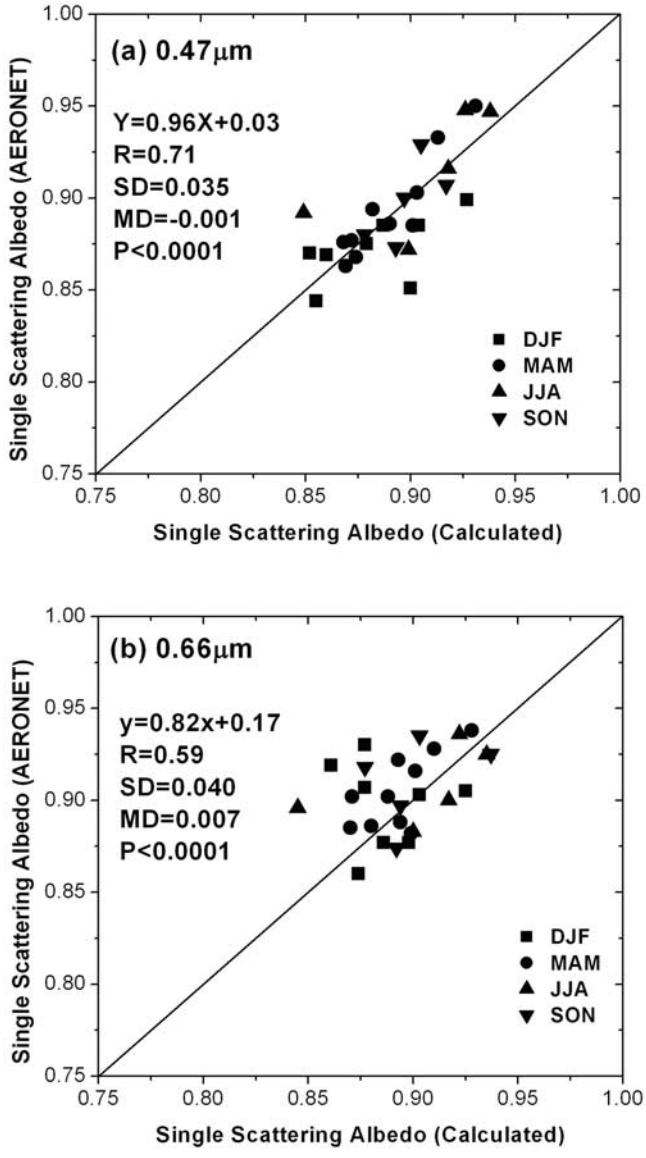

Figure 11. Comparisons of seasonal mean SSAs retrieved from this study and those from the AERONET at four Chinese sites and six international sites.

6. Summary and Conclusion

[35] A new method is proposed here to retrieve aerosol single scattering albedo from a combination of ground-based spectral transmittance and spaceborne TOA reflectance. The method iteratively compares reflected radiances at the TOA as measured by the MODIS with that calculated by the SBDART model using aerosol optical depth data measured on the ground by hazemeters. The method is evaluated against independent retrievals from the AERONET and is applied to generate a SSA database across China during 2005 for high-turbidity conditions (AOT > 0.4).

[36] The sensitivities of the PSD and surface reflectance on SSA retrievals are estimated by means of radiative transfer modeling with the SBDART. Generally, the uncertainty in SSA decreases as AOT increases. The decreasing rates ($\Delta\omega_0/\omega_0 \times 100$) due to the use of different size distribution functions (lognormal versus Junge power law) corresponding to a 50% increase in AOT are 40 $\sim$ 78% (CA), 33 $\sim$ 47% (DD), and 5 $\sim$ 28% (MC), respectively. The sensitivity test to surface reflectance shows a high dependence on the SSA retrieval. The decreasing rate of SSA by a ±0.01 change in surface reflectance are 67 $\sim$ 70% (CA), 67 $\sim$ 73%(UB), 64 $\sim$ 68%(DD), and 68 $\sim$ 69(MC).

[37] The SSA values retrieved by our method agree with those derived by the AERONET inversion algorithm to within the retrieval uncertainties, with SD ranging from 0.019 to 0.046 and MD ranging from −0.011 $\sim$ 0.019 at 0.47 μm, and SD and MD ranging from 0.020 $\sim$ 0.049 and −0.017 $\sim$ 0.029 at 0.66 μm respectively. SSA was estimated at 24 hand-held Sun photometers (hazemeters) stations distributed across China in different ecosystems. The retrieved SSA are analyzed together with AOT and the Ångström exponent. In urban areas, aerosols are relatively small in size and are very absorbing. In desert areas, aerosols are large and moderately absorbing. The average values of AOT, Ångström exponent, and SSA (0.55 μm) over the entire study area in 2005 are 0.69 ± 0.17, 1.06 ±

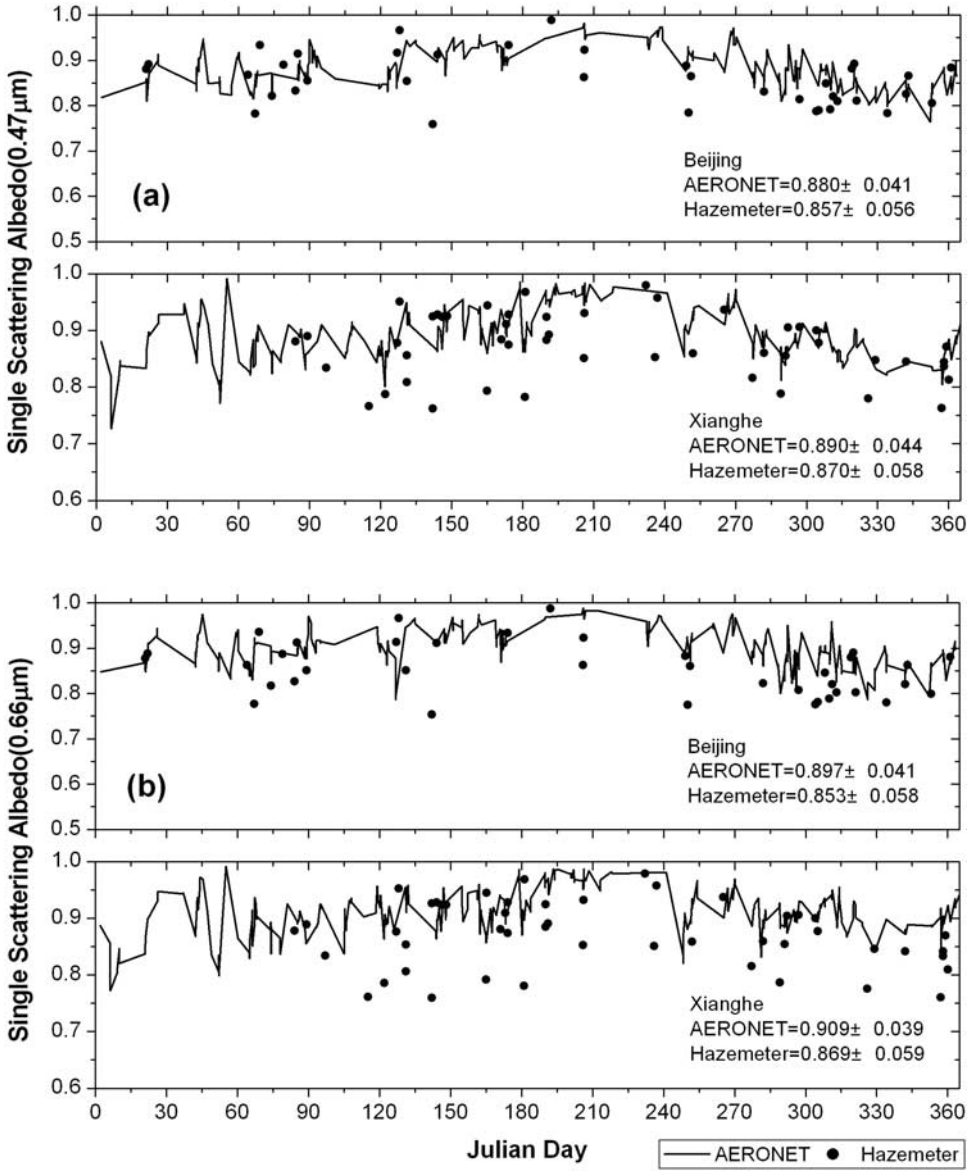

Figure 12. One-year time series of SSA at Beijing and Xianghe at (a) 0.47 μm and (b) 0.66 μm from AERONET (lines) and from this study at the two channels and two locations.

Table 5. Seasonal and Annual Means of AOT, Ångström Exponent, and SSA (550 nm) at the Ground Measurement Sites

Site	Ecosystem	Index	DJF	MAM	JJA	SON	2005
Beijing	urban	τ_{550} (α)	0.90(1.44)	0.60(1.35)	0.97(1.00)	0.70(1.53)	0.79(1.33)
Beijing	urban	ω_0	0.88	0.87	0.93	0.83	0.88
Lanzhou	urban	τ_{550} (α)	1.03(0.73)	0.71(0.98)	0.65(1.03)	0.88(1.17)	0.82(0.98)
Lanzhou	urban	ω_0	0.9	0.89	0.9	0.86	0.89
Shanghai	urban	τ_{550} (α)	0.56(1.27)	0.67(1.10)	0.63(0.92)	0.74(1.17)	0.65(1.12)
Shanghai	urban	ω_0	0.85	0.9	0.89	0.85	0.87
Xianghe	urban	τ_{550} (α)	0.74(1.19)	0.62(1.00)	0.99(0.93)	0.67(1.03)	0.76(1.04)
Xianghe	urban	ω_0	0.83	0.87	0.9	0.86	0.87
Taibei	urban	τ_{550} (α)	NA	NA	0.81(1.14)	NA	0.81(1.14)
Taibei	urban	ω_0	NA	NA	0.83	NA	0.83
Ansai	agriculture	τ_{550} (α)	0.71(2.10)	0.64(0.91)	0.45(0.76)	0.52(1.12)	0.58(1.22)
Ansai	agriculture	ω_0	0.77	0.91	0.9	0.81	0.85
Fenqiu	agriculture	τ_{550} (α)	0.67(1.17)	0.67(0.92)	0.95(0.97)	0.63(1.08)	0.73(1.04)
Fenqiu	agriculture	ω_0	0.89	0.93	0.92	0.91	0.91
Hailun	agriculture	τ_{550} (α)	NA	NA	0.40(1.31)	0.41(1.33)	0.41(1.32)
Hailun	agriculture	ω_0	NA	NA	0.86	0.75	0.81
Shenyang	agriculture	τ_{550} (α)	0.75(1.10)	0.68(1.00)	0.71(0.85)	0.67(1.11)	0.70(1.02)
Shenyang	agriculture	ω_0	0.98	0.86	0.89	0.83	0.89
Taoyuan	agriculture	τ_{550} (α)	0.74(1.21)	0.89(1.00)	0.80(0.92)	0.96(1.14)	0.85(1.07)
Taoyuan	agriculture	ω_0	0.87	0.87	0.91	0.89	0.89
Yanting	agriculture	τ_{550} (α)	0.90(1.08)	0.99(1.00)	0.94(1.15)	0.88(1.03)	0.93(1.07)
Yanting	agriculture	ω_{550}	0.88	0.9	0.87	0.9	0.89
Beijing Forest	forest	τ_{550} (α)	0.50(1.20)	0.77(0.55)	0.75(1.05)	0.58(1.15)	0.65(0.99)
Beijing Forest	forest	ω_0	0.94	0.92	0.88	0.89	0.96
Dinghu Mt.	forest	τ_{550} (α)	0.55(1.17)	NA	NA	0.77(0.97)	0.66(1.07)
Dinghu Mt.	forest	ω_0	0.78	NA	NA	0.9	0.91
Xishuang-banna	forest	τ_{550} (α)	0.74(1.74)	0.77(1.56)	NA	0.44(1.53)	0.65(1.61)
Xishuang-banna	forest	ω_0	0.81	0.83	NA	0.8	0.81
Eerduosi	desert	τ_{550} (α)	NA	0.56(0.42)	NA	0.42(0.85)	0.49(0.64)
Eerduosi	desert	ω_0	NA	0.96	NA	0.95	0.96
Fukang	desert	τ_{550} (α)	NA	NA	0.58(1.35)	0.62(1.28)	0.60(1.32)
Fukang	desert	ω_0	NA	NA	0.95	0.86	0.91
Shapotou	desert	τ_{550} (α)	0.51(0.84)	0.49(0.59)	0.55(0.68)	0.48(0.86)	0.51(0.74)
Shapotou	desert	ω_0	0.88	0.94	0.92	0.86	0.9
Sanjiang	marsh	τ_{550} (α)	NA	NA	0.43(0.93)	0.43(1.34)	0.43(1.13)
Sanjiang	marsh	ω_0	NA	NA	0.99	0.89	0.94
Jiaozhou Bay	bay	τ_{550} (α)	0.70(1.24)	0.86(0.97)	1.10(0.94)	0.88(1.12)	0.89(1.07)
Jiaozhou Bay	bay	ω_0	0.87	0.88	0.92	0.87	0.89
Tai Lake	lake	τ_{550} (α)	0.52(1.01)	0.54(0.81)	0.56(0.65)	0.54(0.91)	0.54(0.85)
Tai Lake	lake	ω_0	0.9	0.95	0.98	0.91	0.94
Average		τ_{550} (α)	0.70(1.22)	0.70(0.94)	0.72(0.98)	0.64(1.13)	0.69(1.07)
Average		ω_0	0.87	0.90	0.91	0.86	0.89

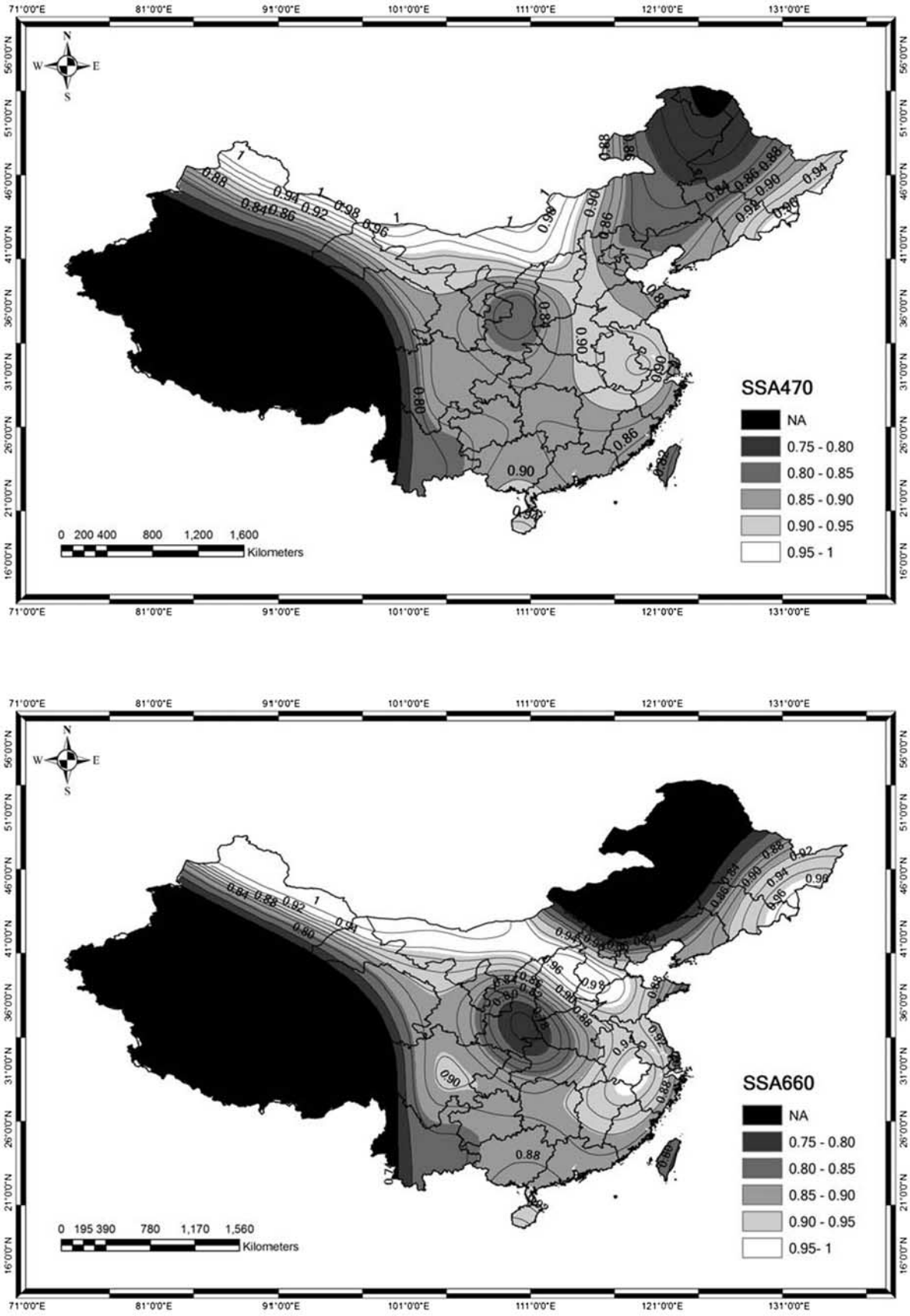

Figure 13. Spatial distribution of retrieved SSA at 0.47 μm and at 0.66 μm over the study area.

0.26, and 0.89 ± 0.04, respectively. This suggests that the aerosols in China have a significant impact on the regional atmospheric environment, and can substantially alter atmospheric heating profiles. Further investigation is needed to validate the retrieved SSA data using other in situ, surface and airborne measurements, and to study the climatic effects of these aerosols.

[38] **Acknowledgments.** This work was supported by the NASA Radiation Science Program (NNG04GE79G), the National Science Foundation (IIS0611892, ATM425069), the National Science Foundation of China (40250120071, 40637035, 40675073), the 973 National Basic Research Program of China (2006CB403706), and the Korean Research Foundation Grant funded by the Korean Government (MOEHRD) (KRF-2006-611-C00009).

References

Ackerman, P., and O. B. Toon (1981), Absorption of visible radiation in atmosphere containing mixtures of absorbing and nonabsorbing particles, *Appl. Opt.*, *20*, 3661–3668.

Ackerman, S. A., K. Strabala, P. Menzel, R. Frey, C. Moeller, L. Gumley, B. Baum, S. W. Seeman, and H. Zhang (1998), Discriminating clear-sky from cloud with MODIS. Algorithm theoretical basis document (MOD35), *J. Geophys. Res.*, *103*(D24), 32,141–32,157.

Bohren, C. F., and D. R. Hoffman (1983), *Absorption and Scattering of Light by Small Particles*, John Wiley, New York.

Brooks, D. R., and F. M. Mims III (2001), Development of an inexpensive handheld LED-based Sun photometer for the GLOBE program, *J. Geophys. Res.*, *106*(D5), 4733–4740.

Bucholtz, A. (1995), Rayleigh-scattering calculations for the terrestrial atmosphere, *Appl. Opt.*, *34*, 2765–2773.

Devaux, C., A. Vermeulen, J. L. Deuze, P. Dubuisson, M. Herman, R. Santer, and M. Verbrugghe (1998), Retrieval of aerosol single scattering albedo from ground-based measurements: Application to observational data, *J. Geophys. Res.*, *103*, 8753–8761.

Dubovik, O., and M. D. King (2000), A flexible inversion algorithm for retrieval of aerosol optical properties from Sun and sky radiance measurements, *J. Geophys. Res.*, *105*(D16), 20,673–20,696.

Dubovik, O., S. Smirnov, B. N. Holben, M. D. King, Y. J. Kaufman, T. F. Eck, and I. Slutsker (2000), Accuracy assessment of aerosol optical properties retrieved from AERONET Sun and sky radiance measurements, *J. Geophys. Res.*, *105*(D8), 9791–9806.

Dubovik, O., B. Holben, T. F. Eck, A. Smirnov, Y. J. Kaufman, M. D. King, D. Tanré, and I. Slutsker (2002), Variability of absorption and optical properties of key aerosol types observed in worldwide locations, *J. Atmos. Sci.*, *59*, 590–608.

Hansen, J. E., and L. D. Travis (1974), Light scattering in planetary atmosphere, *Space Sci. Rev.*, *16*, 527–610.

Hansen, J. E., M. Sato, and R. Ruedy (1997), Radiative forcing and climate response, *J. Geophys. Res.*, *102*, 6831–6864.

Hao, W. M., D. E. Ward, R. A. Susott, R. E. Babbitt, B. L. Nordgren, Y. J. Kaufman, B. N. Holben, and D. M. Giles (2005), Comparison of aerosol optical thickness measurements by MODIS, AERONET sun photometers, and Forest Service handheld sun photometers in southern Africa during the SAFARI 2000 campaign, *Int. J. Remote Sens.*, *26*, 4169–4183.

Haywood, J. M., and V. Ramaswamy (1998), Global sensitivity studies of the direct radiative forcing due to anthropogenic sulfate and black carbon aerosols, *J. Geophys. Res.*, *103*(D6), 6043–6058.

Herman, B. M., R. S. Browning, and J. J. DeLuisi (1975), Determination of the effective imaginary term of the complex refractive index of atmospheric dust by remote sensing: the diffuse-to-direct radiation method, *J. Atmos. Sci.*, *32*, 918–925.

Hess, M., P. Koepke, and I. Schult (1998), Optical properties of aerosols and clouds: The software package OPAC, *Bull. Am. Meteorol. Soc.*, *79*, 831–844.

Hirsch, R. M., and E. J. Gilroy (1984), Methods of fitting a straight line to data: examples in water resources, *Water Resour. Bull.*, *20*, 705–711.

Hu, R.-M., R. V. Martin, and T. D. Fairlie (2007), Global retrieval of columnar aerosol single scattering albedo from space-based observations, *J. Geophys. Res.*, *112*, D02204, doi:10.1029/2005JD006832.

Huang, J., P. Minnis, B. Lin, T. Wang, Y. Yi, Y. Hu, S. Sun-Mack, and K. Ayers (2006), Possible influences of Asian dust aerosols on cloud properties and radiative forcing observed from MODIS and CERES, *Geophys. Res. Lett.*, *33*, L06824, doi:10.1029/2005GL024724.

Huebert, B. J., T. Bates, P. B. Russell, G. Shi, Y. J. Kim, K. Kawamura, G. Carmichael, and T. Nakajima (2003), An overview of ACE-Asia: Strategies for quantifying the relationships between Asian aerosols and their climatic impacts, *J. Geophys. Res.*, *108*(D23), 8633, doi:10.1029/2003JD003550.

Jeong, M.-J., Z. Li, E. Andrews, and S.-C. Tsay (2007), Effect of aerosol humidification on the column aerosol optical thickness over the Atmospheric Radiation Measurement Southern Great Plains site, *J. Geophys. Res.*, *112*, D10202, doi:10.1029/2006JD007176.

Kapustin, V. N., A. D. Clarke, Y. Shinozuka, S. Howell, V. Brekhovskikh, T. Nakajima, and A. Higurashi (2006), On the determination of a cloud condensation nuclei from satellite: Challenges and possibilities, *J. Geophys. Res.*, *111*, D04202, doi:10.1029/2004JD005527.

Kaufman, Y. J. (1987), Satellite sensing of aerosol absorption, *J. Geophys. Res.*, *92*, 4307–4317.

Kaufman, Y. J., A. E. Wald, L. A. Remer, B. C. Gao, R. R. Li, and L. Flynn (1997), The MODIS 2.1-μm channel correlation with visible reflectance for use in remote sensing of aerosol, *IEEE Trans. Geosci. Remote Sens.*, *35*, 1286–1298.

Kaufman, Y. J., J. V. Martins, L. A. Remer, M. R. Schoeberl, and M. A. Yamasoe (2002), Satellite retrieval of aerosol absorption over the oceans using sunglint, *Geophys. Res. Lett.*, *29*(19), 1928, doi:10.1029/2002GL015403.

Kovacs, T. (2006), Comparing MODIS and AERONET aerosol optical depth at varying separation distances to assess ground-based validation strategies for spaceborne lidar, *J. Geophys. Res.*, *111*, D24203, doi:10.1029/2006JD007349.

Krotkov, N. A., P. K. Bhartia, J. Herman, J. Slusser, G. Scott, G. Labow, A. Vasilkov, T. Eck, O. Dubovik, and B. Holben (2005), Aerosol UV absorption experiment (2002–04): 2. Absorption optical thickness, refractive index, and single scattering albedo, *Opt. Eng.*, *44*(4), 041005.

Lee, K. H., Y. J. Kim, and W. von Hoyningen-Huene (2004), Estimation of aerosol optical thickness over northeast Asia from Sea-Viewing Wide Field-of-View Sensor (SeaWiFS) data during the 2001 ACE-Asia intensive observation period, *J. Geophys. Res.*, *109*, D19S16, doi:10.1029/2003JD004126.

Lee, K. H., J. E. Kim, Y. J. Kim, J. Kim, and W. von Hoyningen-Huene (2005), Impact of smoke aerosol from Russian forest fires on atmospheric environment over Korea during May 2003, *Atmos. Environ.*, *39*, 85–99.

Lee, K. H., Y. J. Kim, and M. J. Kim (2006), Characteristics of aerosol observed during two severe haze events over Korea in June and October 2004, *Atmos. Environ.*, *40*(27), 5146–5155.

Lee, K. H., Y. J. Kim, W. von Hoyningen-Huene, and J. P. Burrow (2007), Spatio-temporal variability of satellite-derived aerosol optical thickness over northeast Asia in 2004, *Atmos. Environ.*, *41*(19), 3959–3973, doi:10.1016/j.atmosenv.2007.01.048.

Levy, R. C., L. A. Remer, S. Mattoo, E. F. Vermote, and Y. J. Kaufman (2007), Second-generation operational algorithm: Retrieval of aerosol properties over land from inversion of Moderate Resolution Imaging Spectroradiometer spectral reflectance, *J. Geophys. Res.*, *112*, D13211, doi:10.1029/2006JD007811.

Li, F., and K. Okada (1999), Diffusion and modification of marine aerosol particles over the coastal areas in China: A case study using a single particle analysis, *J. Atmos. Sci.*, *56*(2), 241–248.

Li, Z., et al. (2007a), Aerosol optical properties and their radiative effects in northern China, *J. Geophys. Res.*, *112*, D22S01, doi:10.1029/2006JD007382.

Li, Z., F. Niu, K. H. Lee, J. Xin, W. Hao, B. Nordgren, Y. Wang, and P. Wang (2007b), Validation and understanding of Moderate Resolution Imaging Spectroradiometer aerosol products using ground-based measurements from the handheld Sun photometer network in China, *J. Geophys. Res.*, doi:10.1029/2007JD008479, in press.

Menon, S., J. Hansen, L. Nazarenko, and Y. Luo (2002), Climate effects of black carbon aerosols in China and India, *Science*, *297*, 2250–2252.

Mishchenko, M. I., and L. D. Travis (1998), Capabilities and limitations of a current Fortran implementation of the *T*-matrix method for randomly oriented rotationally symmetric scatterers, *J. Quant. Spectrosc. Radiat. Transfer*, *60*, 309–324.

Moosmüller, H., W. P. Arnott, C. F. Rogers, J. C. Chow, C. A. Frazier, L. E. Sherman, and D. L. Dietrich (1998), Photoacoustic and filter measurements related to aerosol light absorption during the Northern Front Range Air Quality Study (Colorado 1996/1997), *J. Geophys. Res.*, *103*, 28,149–28,157.

Petters, J. L., V. K. Saxena, J. R. Slusser, B. N. Wenny, and S. Madronich (2003), Aerosol single scattering albedo retrieved from measurements of surface UV irradiance and a radiative transfer model, *J. Geophys. Res.*, *108*(D9), 4288, doi:10.1029/2002JD002360.

Qiu, J., L. Yang, and X. Zhang (2004), Characteristics of the imaginary part and single-scattering albedo of urban aerosols in northern China, *Tellus, Ser. B*, *56*, 276–284.

Radke, L. F., D. A. Hegg, P. V. Hobbs, J. D. Nance, J. E. Lyons, K. K. Laursen, R. E. Weiss, P. J. Riggan, and D. E. Ward (1991), Particulate

and trace gas emissions from large biomass fires in North America, in *Global Biomass Burning: Atmospheric, Climatic, and Biospheric Implications*, edited by J. S. Levine, pp. 209–224, MIT Press, Cambridge, Mass.

Ramanathan, V., et al. (2001), Indian Ocean Experiment: An integrated analysis of the climate forcing and effects of the great Indo-Asian haze, *J. Geophys. Res.*, *106*, 28,371–28,398.

Ricchiazzi, P., S. Yang, C. Gautier, and D. Sowle (1998), SBDART: A research and teaching software tool for plane-parallel radiative transfer in the Earth's atmosphere, *Bull. Am. Meteorol. Soc.*, *79*(10), 2101–2114.

Seinfeld, J. H., et al. (2004), ACE-ASIA—Regional climatic and atmospheric chemical effects of Asian dust and pollution, *Bull. Am. Meteorol. Soc.*, *85*(3), 367–380.

Stamnes, K., S.-C. Tsay, W. Wiscombe, and K. Jayaweera (1988), Numerically stable algorithm for discrete-ordinate-method radiative transfer in multiple scattering and emitting layered media, *Appl. Opt.*, *27*, 2502–2509.

Streets, D. G., S. K. Guttikunda, and G. R. Carmichael (2000), The growing contribution of sulfur emissions from ships in Asian waters, *Atmos. Environ.*, *34*, 4425–4439.

Takemura, T., T. Nakajima, A. Higurashi, S. Ohta, and N. Sugimoto (2003), Aerosol distributions and radiative forcing over the Asian Pacific region simulated by Spectral Radiation-Transport Model for Aerosol Species (SPRINTARS), *J. Geophys. Res.*, *108*(D23), 8659, doi:10.1029/2002JD003210.

Torres, O., P. K. Bhartia, A. Sinyuk, E. J. Welton, and B. Holben (2005), Total Ozone Mapping Spectrometer measurements of aerosol absorption from space: Comparison to SAFARI 2000 ground-based observations, *J. Geophys. Res.*, *110*, D10S18, doi:10.1029/2004JD004611.

Wang, M., and H. R. Gordon (1993), Retrieval of the columnar aerosol phase function and single-scattering albedo from sky radiance over the ocean: simulations, *Appl. Opt.*, *32*, 4598–4609.

Wendisch, M., S. Mertes, A. Ruggaber, and T. Nakajima (1996), Vertical profiles of aerosol and radiation and the influence of a temperature inversion: Measurements and radiative transfer calculations, *J. Appl. Meteorol.*, *35*, 1703–1715.

Wenig, M., N. Spichtinger, A. Stohl, G. Held, S. Beirle, T. Wagner, B. Jähne, and U. Platt (2003), Intercontinental transport of nitrogen oxide pollution plumes, *Atmos. Chem. Phys.*, *3*, 387–393.

Xin, J., et al. (2007), Aerosol optical depth (AOD) and Ångström exponent of aerosols observed by the Chinese Sun Hazemeter Network from August 2004 to September 2005, *J. Geophys. Res.*, *112*, D05203, doi:10.1029/2006JD007075.

Yamasoe, M. A., C. von Randow, A. O. Manzi, J. S. Schafer, T. F. Eck, and B. N. Holben (2006), Effect of smoke and clouds on the transmissivity of photosynthetically active radiation inside the canopy, *Atmos. Chem. Phys.*, *6*, 1645–1656.

Yang, H., and H. R. Gordon (1998), Retrieval of the columnar aerosol phase function and single-scattering albedo from sky radiance over land: Simulations, *Appl. Opt.*, *37*, 978–997.

Zhao, F., and Z. Li (2007), Estimation of aerosol single scattering albedo from solar direct spectral radiance and total broadband irradiances measured in China, *J. Geophys. Res.*, *112*, D22S03, doi:10.1029/2006JD007384.

W.-M. Hao, Fire Science Research Lab, Forestry Service, U.S. Department of Agriculture, Missoula, MT 59808, USA.

K. H. Lee, Z. Li, and M. S. Wong, Earth System Science Interdisciplinary Center, Department of Atmospheric and Oceanic Science, University of Maryland, College Park, MD 20742, USA. (kwonlee@umd.edu)

Y. Wang and J. Xin, Institute of Atmospheric Physics, Chinese Academy of Sciences, Beijing 100029, China.

F. Zhao, National Satellite Meteorological Center, China Meteorological Administration, Beijing 100081, China.